

# A new quadruple gravitational lens from the Hyper Suprime-Cam Survey: the puzzle of HSC J115252+004733

Anupreeta More,<sup>1\*</sup> Chien-Hsiu Lee,<sup>2</sup> Masamune Oguri,<sup>1,3,4</sup> Yoshiaki Ono,<sup>5</sup> Sherry H. Suyu,<sup>6,7</sup> James H. H. Chan,<sup>7,8</sup> John D. Silverman,<sup>1</sup> Surhud More,<sup>1</sup> Andreas Schulze,<sup>1</sup> Yutaka Komiyama,<sup>9,10</sup> Yoshiki Matsuoka,<sup>9</sup> Satoshi Miyazaki,<sup>9,10</sup> Tohru Nagao,<sup>11</sup> Masami Ouchi,<sup>5</sup> Philip J. Tait,<sup>12</sup> Manobu M. Tanaka,<sup>13</sup> Masayuki Tanaka,<sup>9</sup> Tomonori Usuda<sup>9,10</sup> and Naoki Yasuda<sup>1</sup>

<sup>1</sup> Kavli Institute for the Physics and Mathematics of the Universe (Kavli IPMU, WPI), University of Tokyo, Chiba 277-8583, Japan

<sup>2</sup> Subaru Telescope, National Astronomical Observatory of Japan, 650 North Aohoku Place, Hilo, HI 96720, USA

<sup>3</sup> Research Center for the Early Universe, University of Tokyo, 7-3-1 Hongo, Bunkyo-ku, Tokyo 113-0033, Japan

<sup>4</sup> Department of Physics, University of Tokyo, 7-3-1 Hongo, Bunkyo-ku, Tokyo 113-0033, Japan

<sup>5</sup> Institute for Cosmic Ray Research, The University of Tokyo, 5-1-5 Kashiwa-no-Ha, Kashiwa City, Chiba, 277-8582, Japan

<sup>6</sup> Max-Planck-Institut für Astrophysik, Karl-Schwarzschild-Str. 1, 85748 Garching, Germany

<sup>7</sup> Institute of Astronomy and Astrophysics, Academia Sinica, P.O. Box 23-141, Taipei 10617, Taiwan

<sup>8</sup> Department of Physics, National Taiwan University, Taipei 10617, Taiwan

<sup>9</sup> National Astronomical Observatory of Japan, 2-21-1 Osawa, Mitaka, Tokyo 181-8588, Japan

<sup>10</sup> SOKENDAI (The Graduate University for Advanced Studies), Osawa, Mitaka, Tokyo 181-8588, Japan

<sup>11</sup> Research Center for Space and Cosmic Evolution, Ehime University, Bunkyo-cho 2-5, Matsuyama, Ehime 790-8577, Japan

<sup>12</sup> Subaru Telescope, 650 North Aohoku Place, Hilo, HI 96720, USA

<sup>13</sup> High Energy Accelerator Research Organization, Institute of Particle and Nuclear Studies, KEK, 1-1 Oho, Tsukuba, Ibaraki 305-0801, Japan

6 February 2017

## ABSTRACT

We report the serendipitous discovery of a quadruply lensed source at  $z_s = 3.76$ , HSC J115252+004733, from the Hyper Suprime-Cam (HSC) Survey. The source is lensed by an early-type galaxy at  $z_l = 0.466$  and a satellite galaxy. Here, we investigate the properties of the source by studying its size and luminosity from the imaging and the luminosity and velocity width of the Ly- $\alpha$  line from the spectrum. Our analyses suggest that the source is most probably a low-luminosity active galactic nucleus (LLAGN) but the possibility of it being a compact bright galaxy (e.g., a Lyman- $\alpha$  emitter or Lyman Break Galaxy) cannot be excluded. The brighter pair of lensed images appears point-like except in the HSC  $i$ -band (with a seeing  $\sim 0''.5$ ). The extended emission in the  $i$ -band image could be due to the host galaxy underneath the AGN, or alternatively, due to a highly compact lensed galaxy (without AGN) which appears point-like in all bands except in  $i$ -band. We also find that the flux ratio of the brighter pair of images is different in the Ks-band compared to optical wavelengths. Phenomena such as differential extinction and intrinsic variability cannot explain this chromatic variation. While microlensing from stars in the foreground galaxy is less likely to be the cause, it cannot be ruled out completely. If the galaxy hosts an AGN, then this represents the highest redshift quadruply imaged AGN known to date, enabling study of a distant LLAGN. Discovery of this unusually compact and faint source demonstrates the potential of the HSC survey.

**Key words:** gravitational lensing: strong – methods: observational – quasars: individual

## 1 INTRODUCTION

Strong gravitational lensing is a powerful astrophysical and cosmological tool. Gravitational lenses act as natural telescopes to provide

\* anupreeta.more@ipmu.jp

a sneak peek at some of the most distant and faintest galaxies and quasars in the Universe.

Distant galaxies are mostly comprised of star-forming galaxies (SFGs) often identified in observations as Lyman Break Galaxies (LBGs) or Lyman- $\alpha$  emitters (LAEs). The magnification due to gravitational lensing is critical to study the faint end of the distant LAE and LBG populations at high angular resolution. Lensing has enabled several studies such as sources of cosmic reionization (e.g., Stark et al. 2007; Atek et al. 2015), understanding the physical properties of LAEs/LBGs at high redshifts  $z = 6 - 7$  (e.g., Egami et al. 2005; Bradley et al. 2008; Huang et al. 2016), their molecular gas and inter-stellar medium (ISM) properties (e.g., Riechers et al. 2010; Rawle et al. 2014) as well as their abundances (e.g., Bradley et al. 2014; Schmidt et al. 2016).

Lensed quasars have also proven to be useful as both cosmological and astrophysical probes. For example, the time delays provide a direct way to measure cosmological parameters (e.g., Suyu et al. 2016) and source reconstruction of lensed quasars and their host gives a direct view on the co-evolution of quasars and host galaxies (e.g., Peng et al. 2002; Rusu et al. 2016). Systematic searches for lensed quasars have successfully found over a hundred lens systems, in the radio (e.g., Myers et al. 2003; Browne et al. 2003), in the optical (e.g., Oguri et al. 2006; Inada et al. 2012; More et al. 2016) as well as other multi-wavelength regimes (e.g., Jackson et al. 2012). On galaxy scales, lensed quasars are typically doubly imaged (“doubles”) or quadruply imaged (“quads”). Most of the lensed quasar systems discovered to date are doubles. For example, a sample of thirteen lensed quasars recently discovered by More et al. (2016) from the Sloan Digital Sky Survey (SDSS) -III are all doubles. Nonetheless, quads with their two additional images provide additional astrophysical information on the foreground lens and the background source. Finding more quad quasar lenses is thus of tremendous value to the community given the small number<sup>1</sup> of currently known quads.

In this paper, we report the discovery of the quad lens HSC J115252+004733 (henceforth referred to as HSC J1152+0047) from the Hyper Suprime-Cam (HSC) Survey. The HSC Survey is a Subaru Strategic Program (SSP) using the newly installed HSC (Miyazaki et al. 2012) instrument on the Subaru 8.2-m telescope. The survey consists of three layers (wide, deep, ultradeep), where the wide layer is expected to cover  $\sim 1400 \text{ deg}^2$  in *grizY*-bands down to a depth of  $r \sim 26$ . The HSC data are processed with hscPipe, which is derived from the LSST software pipeline (Ivezic et al. 2008; Axelrod et al. 2010; Jurić et al. 2015), and are calibrated using the Pan-STARRS1 data (Tonry et al. 2012; Schlafly et al. 2012; Magnier et al. 2013).

Our paper is organized as follows. In Section 2, we describe the discovery of HSC J1152+0047 and the multi-wavelength imaging data on this lens system. We describe the spectroscopic follow-up in Section 3. The lens mass modeling is described in Section 4. In Section 5, we derive the properties of the delensed source. In Section 6, we compare our source with other distant galaxies and quasars to understand its nature and discuss the cause of chromatic variation in flux ratios. We present our conclusions in Section 7. Magnitudes quoted in this paper are in AB magnitudes unless otherwise stated. The terms active galactic nuclei (AGN) and quasar may

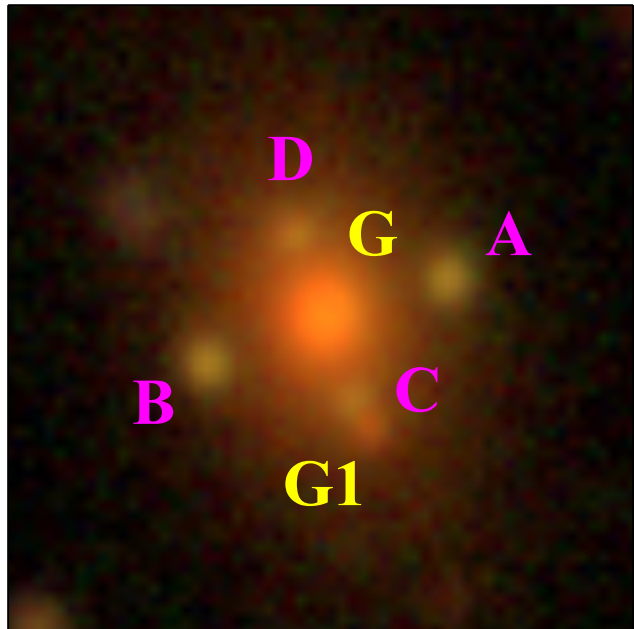


**Figure 1.** Color (*gri*) composite of HSC J1152+0047 showing the four blue lensed images (A, B, C and D) in an Einstein-cross configuration. Apart from the central lensing galaxy (G), a companion galaxy (G1, close to image C) is probably contributing to lensing. The image is  $10''$  on the side. North is up and East is left.

be used interchangeably in the text. We used the following cosmological parameters wherever necessary  $\Omega_m = 0.308$ ,  $h = 0.678$ ,  $\Omega_k = 0$  (Planck Collaboration et al. 2016).

## 2 IMAGING DATA OF HSC J1152+0047

The lens system, HSC J1152+0047, was recently discovered serendipitously during the visual inspection of data from the HSC Wide (internal data release  $\sim 80 \text{ sq. deg.}$ , S15A). HSC J1152+0047 consists of the main lens galaxy (G) with four lensed images (A, B, C and D) in a cross configuration (see Fig. 1). A second galaxy (G1) located very close to image C, is probably a satellite of the main lens galaxy G and is likely to perturb the lens potential.

We measured the relative positions and photometry of the lens galaxies and the lensed images from the HSC imaging using GALFIT (Peng et al. 2002). In Fig. 2, we show all of the HSC bands and the model-subtracted residual images for each band, respectively. The seeing in the HSC-*g*, *r*, *i*, *z* and *Y* images is found to be  $0''.55$ ,  $0''.46$ ,  $0''.45$ ,  $0''.60$ , and  $0''.61$ , respectively, as per hscPipe. All of the four lensed images are fit with a point spread function (PSF) model in all bands except in the *i*-band, where a Sersic profile is better fit to images A and B. The lens galaxy G is fit with a double Sersic model and the companion galaxy G1 is fit with a PSF model. For lens galaxy G, we used the *z*-band best-fit model as prior when fitting the double Sersic model in other bands. The relative positions from *z*-band and photometry in all bands along with errors from GALFIT are given in Table 1. We note that the colors ( $g - r$  and  $r - i$ ) of the lensed images (see Table 1) are consistent with the colors of a quasar at  $z \sim 4$  (Richards et al. 2001).

We find that our system is detected in the near-infrared (NIR) imaging taken by the VISTA Kilo-degree Infrared Galaxy survey (VIKING; Edge et al. 2013). The *JHKs* imaging obtained

<sup>1</sup> According to the Master Lens Database (<http://admin.masterlens.org/index.php>), from a collection of over 115 lensed quasars, about 30 systems are known to be quads.

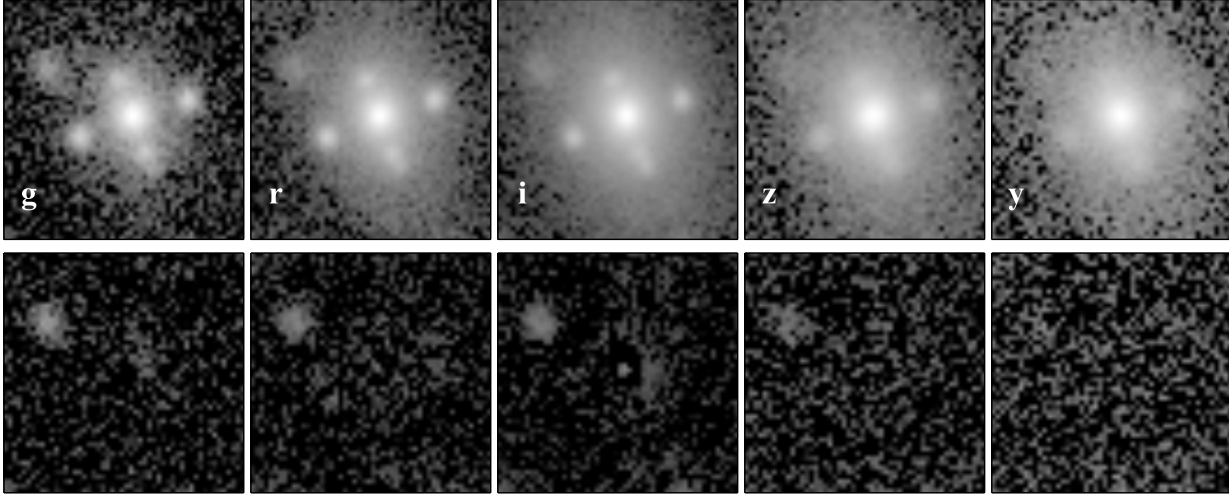


**Figure 2.** GALFIT modeling results in HSC *grizY*-bands. Top panels show the HSC images whereas the bottom panels show GALFIT model subtracted residual images in the respective bands. Images are  $9''$  on the side.

from the VISTA Science Archive (VSA)<sup>2</sup> is shown in Fig. 3. The brighter pair of lensed images shows hints of presence in the *J* and *H* imaging, whereas they are well detected in the *K*s-band. We fit a PSF model to the brighter pair of images and a Sersic model to the galaxy G with GALFIT. We use the 2MASS *K*-band magnitude of a nearby star for the flux calibration of our VIKING *K*s-band photometry. The images A, B and galaxy G have *K*s-band magnitudes of  $19.31 \pm 0.10$ ,  $20.28 \pm 0.27$  and  $15.23 \pm 0.14$  Vega mag, respectively where the reported errors are from GALFIT.

We also checked if the lensed source is detected in the Wide-field Infrared Survey Explorer (WISE) imaging (Wright et al. 2010). While W1- and W2-bands show emission at the center of HSC J1152+0047, we cannot confirm the presence of the lensed source due to source confusion owing to the low resolution ( $6''$ ). The source catalog from WISE reports two detections. One of the sources coincides with the lens galaxy G whereas the second source does not coincide with any of the lensed images or galaxy G1 (see Fig. 3). The lens galaxy G has  $W1 = 15.18 \pm 0.04$  and  $W2 = 15.04 \pm 0.08$  Vega mag, respectively. In bands W3 and W4, there is no detection of any emission either from the lens or the lensed source thus, providing a strong upper limit on source flux. The sensitivities with a signal-to-noise ratio (SNR) of 5 for W3 and W4 bands are 11.5 and 7.87 Vega mag, respectively.

We show the flux ratios of images B, C, D with respect to image A in Fig. 4 for all of the HSC *grizY*-bands and VIKING *K*s-band. All of the three flux ratios appear nearly uniform across the optical bands with no strong evidence for differential reddening. However, the flux ratio of the brighter image pair ( $B/A \sim 0.41 \pm 0.11$ ) in *K*s-band (observed in year 2011) is discrepant with the flux ratio of  $0.95 \pm 0.02$  seen in the HSC data (observed in year 2015). In Section 6.2, we discuss various phenomena that are known to introduce chromatic (i.e. wavelength dependent) variation in the flux ratios of lensed images in the attempt to find plausible explanation for this discrepancy.

Images C and D are detected in the optical bands only. The flux of image C is likely contaminated by the emission from satellite galaxy (G1) in the reddest (*Y*) band where G1 becomes more

**Table 1.** Relative astrometry and photometry of HSC J1152+0047 using GALFIT.

Name	$\Delta x$ err	$\Delta y$ err	<i>g</i> err	<i>r</i> err	<i>i</i> err	<i>z</i> err	<i>Y</i> err
A	0.0	0.0	24.23	23.10	22.82	22.82	22.80
	—	—	0.06	0.02	0.02	0.02	0.04
B	-3.85	-1.34	24.32	23.12	22.87	22.79	22.86
	0.01	0.01	0.06	0.02	0.02	0.02	0.04
C	-1.52	-1.87	24.76	23.71	23.49	23.29	23.50
	0.02	0.02	0.10	0.05	0.03	0.03	0.15
D	-2.45	0.70	24.71	23.61	23.41	23.27	23.19
	0.01	0.01	0.10	0.05	0.03	0.03	0.07
G	-1.96	-0.57	21.85	20.31	19.52	19.15	19.05
	0.01	0.01	0.12	0.05	0.05	0.02	0.03
G	-2.04	-0.47	21.63	20.27	19.43	19.18	19.06
	0.01	0.02	0.22	0.03	0.12	0.03	0.03
G1	-1.25	-2.36	25.87	24.43	23.62	23.22	23.01
	0.01	0.02	0.24	0.07	0.03	0.04	0.11

The position of image A is RA,Dec=(178.21722, 0.79271) deg. The relative astrometry is from the *z*-band in units of arcsec. The positive directions of  $\Delta x$  and  $\Delta y$  are North and West, respectively. For every object, the second row shows the errors from GALFIT. Except the *i*-band for images A and B where a Sersic model is chosen, all of the lensed images are fit with a PSF model. The magnitudes are corrected for Galactic extinction.

prominent (see Fig. 4 and Table 1). In the bluer bands, the fluxes of images C and D are comparable as expected for this image configuration from lensing. Although the presence of G1 could affect the magnification of image C, we do not detect any significant difference between relative fluxes of C and D.

### 3 SPECTROSCOPIC OBSERVATION OF HSC J1152+0047

We obtained spectra of HSC J1152+0047 on 2016 March 11 (Program ID: GN-2016A-FT-7) with Gemini North Telescope through the Fast Turnaround program (Mason et al. 2014) with seeing

<sup>2</sup> <http://horus.roe.ac.uk/vsa/dboverview.html>

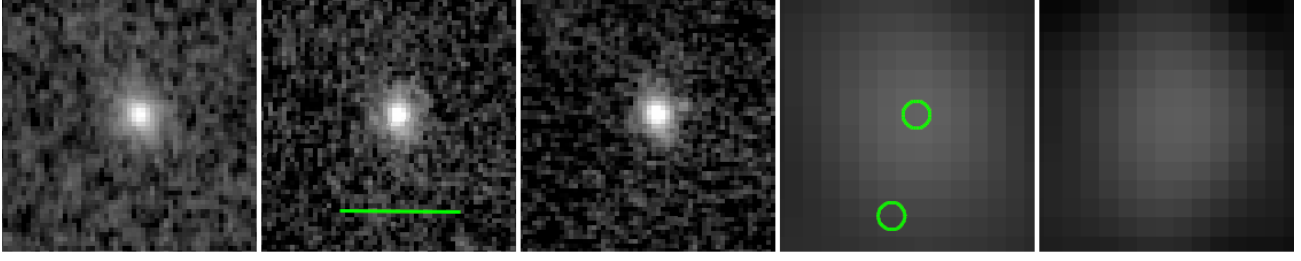


**Figure 3.** From left to right, NIR VIKING imaging in Filters (limiting AB magnitudes)  $J(22.1)$ ,  $H(21.5)$ , and  $Ks(21.2)$  followed by WISE imaging in bands W1 and W2. The brighter pair of lensed images are close to the detection limits of VIKING  $J$  and  $H$  imaging whereas they are detected in the  $Ks$ -band. W1 and W2 imaging show emission from the lens galaxy alone (see Section 2). The two green circles mark the location of sources detected from the WISE catalogs. North is up and East is left. The bar shows a scale of  $9''$ .

around  $0''.6$ – $0''.7$ . We used GMOS in the long-slit mode with R400-G5305 grating and GG455 blocking filter. The width of the slit was set to  $1''.0$ . This provides a spectral resolution  $R=1918$  and wavelength coverage from 4000 to 8000 Å. Two perpendicular slit configurations were used to acquire spectra of all 4 lensed images, as well as the lens galaxy G. The brighter pair was observed for 15 min and the fainter pair was observed for 45 min. The companion galaxy G1 is aligned with the fainter pair and fell on the second slit but was too faint to be detected.

We carried out the data reduction using IRAF with the dedicated GMOS package (v1.13). The spectra were bias subtracted, flat fielded and sky subtracted. We used CuAr lamp to calibrate the wavelength. Because the lensed image spectra are very faint and close to the spectra of the lens galaxy ( $<2''$  for the brighter pair, and  $<1''$  for the fainter pair), we manually select the aperture size and spectra position to extract the lensed image spectra. This is done using the ‘gsextract’ routine in an interactive mode. For the fainter pair, the spectra are dominated by the lens galaxy light. To avoid contamination from the lens for the fainter pair of images, we scaled the red part ( $> 7000$  Å) of the lens spectrum to match the spectrum of the fainter images assuming that most of the redder part is dominated by the emission from the lens. We then subtracted this normalized lens galaxy spectrum from the spectra of the fainter images. We calibrate the flux based on spectroscopic standard star. We estimate flux errors using the variance at each pixel, which is calculated from the raw image, and taking into account the effects of each reduction step using error propagation, till extracting the one-dimensional spectra.

The spectra of the lens galaxy and the four lensed images are shown in Fig. 5. The spectra of each of the lensed images in the figure are smoothed with a Gaussian filter of  $2.7$  Å and vertical offsets are added for illustrative purpose. The redshift of the lens galaxy is found to be  $z_l = 0.466 \pm 0.001$  through the identification of CaII H and K absorption lines near the 4000 Å break as expected for a typical early-type galaxy. As mentioned earlier, we do not have a spectrum of G1 but our photometric redshift estimate ( $z_{lG1} = 0.46 \pm 0.15$ ) suggests that G1 is a gravitationally bound satellite of galaxy G. The similarity in the spectra of the four images confirms the strong lensing nature of this system. The redshift of the lensed source is found to be  $z_s = 3.76 \pm 0.01$  based on the identification of the Ly- $\alpha$  emission line. Also, the stacked spectrum shows other high ionization state lines e.g., NV in emission and C IV in absorption which are rather weak but their presence is consistent with the interpretation of the stronger emission line as Ly- $\alpha$  (see Fig. 5).

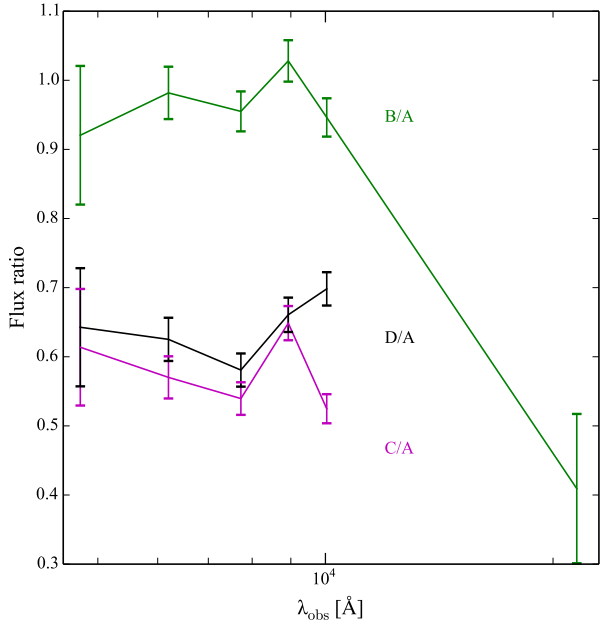


**Figure 4.** Flux ratios of the lensed images as a function of wavelengths in the optical (HSC *grizY*-band, see also Table 1). For the brighter pair of images, we also include the  $Ks$ -band data in the NIR.

#### 4 LENS MASS MODELING

We used the lens modeling software GLAFIC (Oguri 2010) for lens mass modeling. We started with  $i$ -band HSC image where information from each pixel offer data constraints for the mass models.

The lens galaxies are each modeled with an isothermal density profile. Galaxy G is allowed to have ellipticity whereas galaxy G1 is assumed to have spherically symmetric mass distribution since G1 is less massive and the contribution from the quadrupole moment of its mass distribution is not expected to be significant. While we allowed for external shear to be present earlier in our models, we found that this was highly degenerate with the ellipticity of G and did not improve the fit significantly. Hence, we removed it for simplicity. Thus, our final lens mass model consists of an isothermal ellipsoid (SIE) for G and an isothermal sphere (SIS) for G1.

We tested different assumptions when modeling the light profile of the lensed source. Our list of models comprised i) single PSF ii) single Sersic and iii) PSF+Sersic. We found that a single PSF model left significant residuals in the  $i$ -band image, as expected and a PSF+Sersic model was not an improvement over the single

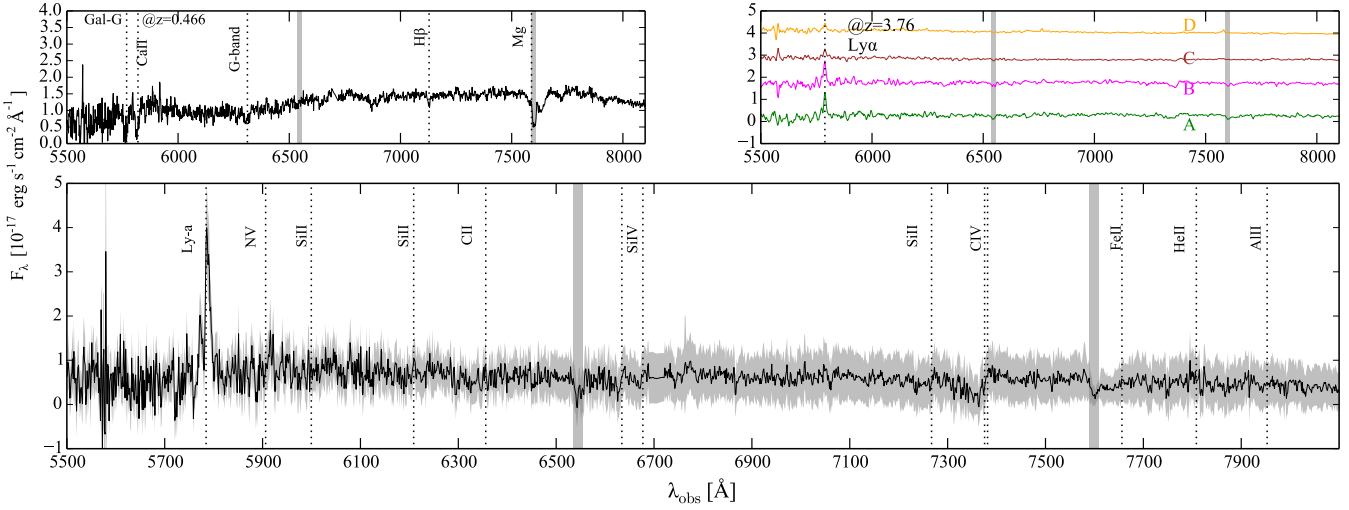


**Figure 5.** *Upper left:* The spectrum of the lensing galaxy from our Gemini GMOS spectroscopic follow-up observation. The lens redshift is  $z_l = 0.466$ . *Upper right:* Individual binned spectra of the lensed images A–D from the Gemini GMOS spectroscopy. All the images have the Ly- $\alpha$  emission line redshifted to  $z_s = 3.76$ . *Lower:* The stacked spectrum of the lensed source with commonly found emission and absorption lines labelled. The error on the spectrum is shown with the shaded region (grey). The two vertical bars (grey) shown in all panels indicate absorption features probably due to telluric contamination.

Sersic model. Therefore, our final best model for the lensed source is a single Sersic component.

We run Monte Carlo Markov Chain (MCMC) using EMCEE (Foreman-Mackey et al. 2013). The model fitting includes pixels within a  $7''$  box centered on the lens (see left panel of Fig. 6). The medians of the posterior distributions of our model parameters are given in Table 2. We only report the source magnitude and effective radius from our model in Table 2 since other source parameters such as the ellipticity and position angle (PA) are not well-constrained. Also, since the Sersic index  $n$  was not well-constrained we fixed it to  $n = 4$  that corresponds to the de Vaucouleurs’ profile.

In Fig. 6, we show the model image (middle panel) and the residual image (right panel) after subtracting the model from the data. We also show critical curves (white contours) and caustics (magenta contours) marking the regions of infinite magnification in the middle panel. We highlight the peak positions of the model-predicted lensed images (circles) and the true source position (triangle).

Finally, we also constructed mass models by fitting to just the peak positions and relative fluxes of the lensed images which were measured with GALFIT. We tested similar lens models as before except that the source is assumed to be a point source since the data constraints are limited. From this analysis, we determined a magnification factor of  $\mu = 2.5 - 3$  for images A and B. We choose  $\mu = 2.5^3$  for the analysis presented in Section 5.

## 5 RESULTS

In this section, we determine the properties of the lensed source based on the modeling of the imaging and spectroscopic data. First, we analyze the single most prominent emission line found in the spectra of the lensed images. Next, we determine the true source

**Table 2.** Mass modeling results from fitting a lensed extended source to  $i$ -band image.

Parameters	Values (units)
Velocity dispersion (G)	$280 \pm 10 \text{ km s}^{-1}$
Ellipticity (G)	$0.54 \pm 0.02$
PA of Ellipticity (G)	$19.1 \pm 0.5 \text{ deg}$
Velocity dispersion (G1)	$100 \pm 30 \text{ km s}^{-1}$
True Source magnitude	$23.9 \pm 0.1$
True Source Effective radius	$0.028 \pm 0.005 \text{ arcsec}$

**Table 3.** Properties of Ly- $\alpha$  for the brighter pair of lensed images.

Name	EW $\text{\AA}$	FWHM $\text{km s}^{-1}$	$L \times 10^{42}$ $\text{ergs s}^{-1}$
A	$16 \pm 1$ (30)	$540 \pm 40$ (920)	3.2 (6.3)
B	$15 \pm 1$ (26)	$640 \pm 50$ (890)	3.2 (6.3)

The values are given for the narrow component of Ly- $\alpha$  and the values within parentheses are given for the broader component. The EW is given in the rest-frame. The luminosities are dereddened by taking into account the magnification factor.

magnitude and size to decide whether the source is dominated by an AGN or not.

### 5.1 Ly- $\alpha$ emission

We fit a Gaussian to the one-dimensional spectrum around the Ly- $\alpha$  emission in images A and B (see Fig. 7). We obtain a line width of  $\sigma = 4.6 \pm 0.3 \text{\AA}$  and  $5.4 \pm 0.4 \text{\AA}$  at  $5788 \text{\AA}$ , respectively. Given the spectral resolution ( $R = 1918$ ), the instrumental broadening corresponds to  $156 \text{ km s}^{-1}$ . Thus, the Full-Width at Half-Maximum (FWHM) of Ly- $\alpha$  emission from images A and B, after

<sup>3</sup> We note that choosing  $\mu = 3$  does not qualitatively change our conclusions about the source properties.



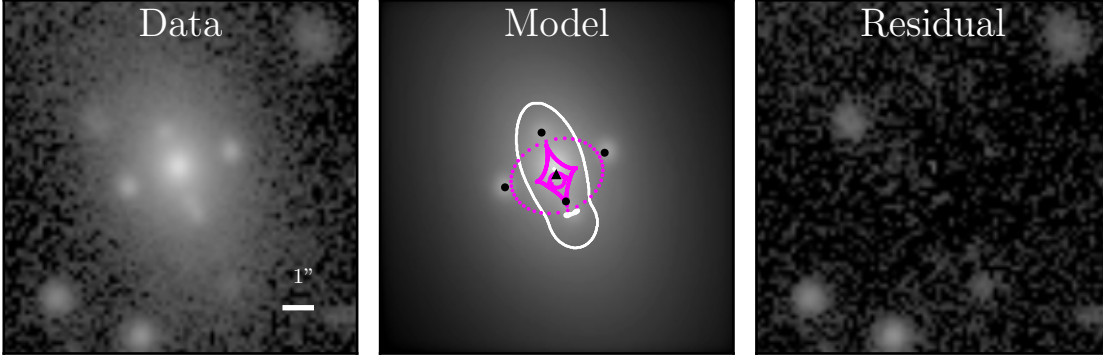


**Figure 6.** HSC *i*-band image (*left*), lens mass model where the background source is assumed to have a Sersic profile (*middle*) and the residual image (*right*). The middle panel also shows the positions of the lensed images (circles) and the source (triangle). The magenta contours show the caustics in the source plane and white contours mark the corresponding critical curves in the image plane indicating regions of extremely high magnification.

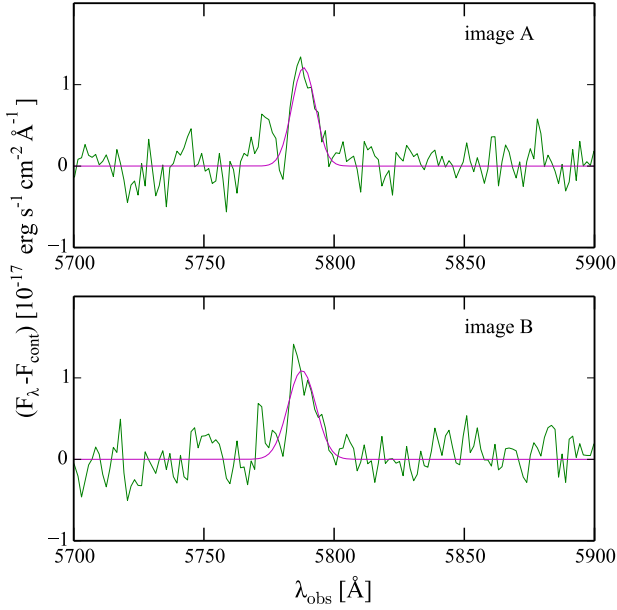


**Figure 7.** One-dimensional Gaussian fit to the continuum subtracted spectrum near the Ly- $\alpha$  feature for image A (*upper*) and image B (*lower*).

accounting for the instrumental broadening, is  $540 \pm 40 \text{ km s}^{-1}$  and  $640 \pm 50 \text{ km s}^{-1}$ , respectively. There is a second peak blueward of the Ly- $\alpha$  line, which suggests that the underlying Ly- $\alpha$  is much broader, with different parts of the emission line modified by absorption or resonant scattering from surrounding neutral hydrogen (e.g. Miralda-Escudé 1998). This absorption feature is more obvious for image A than image B. The FWHMs of the broader Ly- $\alpha$  line (including the second peak to the left) of images A and B are  $\sim 920$  and  $\sim 890 \text{ km s}^{-1}$ , respectively. This is also consistent with the FWHM estimate measured from the stacked (unbinned) spectra of the four images shown in Fig. 5.

The flux of the Ly- $\alpha$  line from a flux-calibrated spectrum of image A is  $1.4 \times 10^{-16} \text{ ergs s}^{-1} \text{ cm}^{-2}$  which gives a luminosity of  $10^{42.5} \text{ ergs s}^{-1}$  after taking into account the magnification factor  $\mu$  of 2.5. The equivalent width (EW) of Ly- $\alpha$  line is  $75 \pm 5 \text{ \AA}$  in the observed frame and  $16 \pm 1 \text{ \AA}$  in the rest frame for image A. The errors represent 68% confidence levels on the posterior distribution

of the parameters sampled with MCMC. We present the measurements for both the narrow and the broad components of Ly- $\alpha$  in Table 3.

## 5.2 Source Magnitude

GALFIT model fitting to image A in the *i*-band suggested  $i = 22.82$ . Using the magnification factor of  $\mu = 2.5$ , we obtain a delensed source magnitude of  $i = 23.84$ . At  $z_s = 3.76$ , this corresponds to an absolute magnitude  $M_{1500} = -22.1$  after applying a K-correction for the continuum  $K_{\text{corr}} = -2.5 (1 + \alpha) \log (1 + z_s) - 2.5 \alpha \log (1500 \text{ \AA} / \lambda_{\text{eff}})$  following the prescription of Glikman et al. (2010) where  $\alpha = -0.5$  (Richards et al. 2006) for quasars.

Alternatively, we can determine the true source magnitude from the results of our lens mass modeling by fitting an extended source to the *i*-band image. The best-fit source magnitude thus obtained, is  $i = 23.9 \pm 0.1$  which corresponds to  $M_{\text{UV}} = -22.0 \pm 0.1$ .

## 5.3 Source size

We followed the same two approaches as before to estimate the true source size. GALFIT model fitting suggested a size of  $r_{\text{eff},l} = 0''.12$  where subscript  $l$  indicates lensed. The lensing magnification factor ( $\mu = 2.5$ ) is used to scale down the area of the lensed source to get the true source size. We assume the source is circular (i.e.  $\text{area} = \pi r_{\text{eff},t}^2$  where subscript  $t$  implies true) and that the lensing magnification is the same in all directions. Thus, the true source size is estimated to be  $r_{\text{eff},t} = \sqrt{r_{\text{eff},l}^2 / \mu} = 0''.069$ . Given the physical scale at  $z_s = 3.76$  of  $7.33 \text{ kpc arcsec}^{-1}$ , the source size is  $\sim 0.56 \text{ kpc}$  in physical units.

The best-fit source size  $r_{\text{eff},t}$  from lens mass modeling is found to be even smaller,  $\sim 0''.028 \pm 0''.005$ , suggesting a physical source size of  $0.20 \pm 0.04 \text{ kpc}$ . We trust our latter estimate more because the former estimate has a larger systematic error owing to the strong assumptions adopted in our calculation.

## 6 DISCUSSION

In this section, we compare properties of high redshift galaxies with the lensed source of HSC J1152+0047 to decide whether the source

has an AGN or not. We also discuss possible sources of chromatic variations seen in the flux ratio of the brighter pair of lensed images.

### 6.1 Comparison with high redshift galaxies

Here, we consider comparison with LAEs and LBGs. LAEs are star-forming galaxies with faint ultra-violet (UV) continuum and a prominent Ly- $\alpha$  emission line (e.g. Malhotra & Rhoads 2002; Ouchi et al. 2008; Shibuya et al. 2012).

LAEs are known to have large  $EW_{Ly-\alpha}$  and small velocity widths  $\Delta v_{Ly-\alpha}$  (e.g., Ouchi et al. 2008; Hashimoto et al. 2013). For example, rest-frame  $EW_{Ly-\alpha}$  for a sample of LAEs at  $z \sim 3.7$  is  $> 44 \text{ \AA}$  (Ouchi et al. 2008) much larger than that of our lensed source but their sample is limited by the selection effects of their narrow-band data. Usually LAEs are defined to be high-redshift galaxies with rest-frame  $EW_{Ly-\alpha} \geq 20 \text{ \AA}$  (e.g., Ouchi et al. 2003). Thus, our source is probably at the border of being an LAE based on the EW criteria. Ouchi et al. (2010) measured velocity widths of Ly- $\alpha$  for a large sample of over 200 Ly- $\alpha$  emitter (LAEs) at high redshifts. They find average velocity widths of  $260 \text{ km s}^{-1}$  without significant difference between  $z = 5.7 - 6.6$ . Assuming that this holds true at  $z \sim 4$ , the FWHM of Ly- $\alpha$  for the source in HSC J1152+0047 is much broader to be an LAE type of galaxy.

The characteristic of LBGs is a sharp drop in the flux bluewards of the Ly- $\alpha$ . We do not see any strong evidence of such a sharp cut-off in either the spectrum (see Fig. 5) or the imaging although its colors may not be inconsistent with an LBG (e.g., Bouwens et al. 2014).

Shibuya et al. (2015) derived the size-magnitude ( $M_{UV}$ ) relation for SFGs and LBGs at  $z \sim 4$  (as shown in Figure 9 of their paper). Our source is an outlier for the  $z \sim 4$  population and does not show expected size and magnitude properties for either SFGs or LBGs at that redshift. In fact, it is extremely compact and at the brighter end of the rest of the population suggesting that the source probably has an AGN with low-to-moderate luminosity.

### 6.2 Chromatic variations in the flux ratios

#### 6.2.1 Intrinsic variability due to AGN

AGNs are known to show intrinsic variability over months to years whereas galaxies do not have any mechanism to produce variability on such time scales, except when they host luminous transients such as supernovae. From the geometrical symmetry of the lensed images in an Einstein cross and from our mass models, the relative time delay in the arrival of light rays between the brighter pair of the lensed images is a few days. The difference of 1 magnitude in the brighter pair (Fig. 4), which are separated by a relative time delay of a few days, is too rapid to be caused by intrinsic flux variation in the AGN.

#### 6.2.2 Microlensing

Microlensing is the lensing effect produced by very low mass compact components, for example, from stars, globular clusters or black holes in the plane of a lens galaxy. Microlensing could produce chromatic variations in flux ratios. This effect is sensitive to the scale of the source size. The size of region emitting rest-frame optical (observed frame NIR) in the source plane is much larger than that of the region emitting rest-frame UV (observed frame optical).

Thus, the  $K$ -band fluxes are expected to be less affected by microlensing. However, HSC J1152+0047 shows a discrepancy in the  $K$ -band flux ratio instead of the optical.

Also, the VIKING  $Z$ -band (not shown here) suggests a flux ratio,  $B/A \sim 1$  consistent with HSC data. The VIKING  $K$ -band data were taken 1 yr after VIKING  $Z$ -band data and HSC data were taken 4 yrs after  $K$ -band data. Ignoring the fact that we are comparing data in different bands here, these timescales even though short are still feasible for microlensing to appear, based on the caustic crossing time estimated by following Treyer & Wambsganss (2004).

Microlensing can also be deduced by comparing the continuum and emission line flux ratios (e.g. Sluse et al. 2007). The ratio of the flux calibrated optical spectra of images A and B is nearly one, both for the continuum and the Ly- $\alpha$  emission line disfavoring the microlensing scenario although the weaker NV and CIV emission lines have different relative strengths but are not reliable. In summary, microlensing cannot be considered as the source of the discrepancy between the optical and NIR flux ratios without additional data. High resolution and deeper spectroscopy is needed to rule out or confirm microlensing with certainty.

#### 6.2.3 Differential Extinction

Extinction from the presence of dust in the lens galaxy could affect the flux ratios as a function of the wavelength. Firstly, the lens galaxy is an early-type galaxy which usually do not have significant dust to cause severe extinction of the lensed images (e.g. Falco et al. 1999; Elíasdóttir et al. 2006). Secondly, we do not see any obvious dust lanes in the deep HSC imaging. Given that the system is fairly symmetrical in the near North-South direction and that images A and B are almost equidistant on the either side of the lens galaxy, the amount of dust is not expected to be significantly different to cause such a high level of differential extinction in the lensed images A and B and in the  $K$ -band alone. Also, extinction affects strongly at shorter wavelengths but the flux ratio,  $B/A$  does not show any sign of extinction in the HSC data. Furthermore, the measured flux ratios in the optical are completely consistent with a simple lens mass model without the need to include any model for the dust extinction. Thus, extinction is unlikely to be the source of chromatic variation seen in HSC J1152+0047.

## 7 CONCLUSION

We have discovered a quadruply imaged source from the HSC survey at  $z_s = 3.76$  lensed by an early-type galaxy at  $z_l = 0.466$ . In this paper, we attempt to understand the whether of the background source has an AGN at its core by considering various observational evidences.

- The Ly- $\alpha$  emission line is narrow but broader than velocity widths typically found in LAEs and LBGs and its luminosity is consistent with a faint AGN. The rest-frame UV spectrum shows weak metal emission lines (NV and blue-wing absorbed C IV) found in the NLR/BLR around AGNs.

- The rest-frame UV absolute magnitude ( $M_{UV} = -22$ ) of the source suggests that it either belongs to the rare population of intrinsically bright galaxy population (e.g., Kobayashi et al. 2010; Parsa et al. 2016) or the very abundant population of faint AGNs (e.g., Glikman et al. 2011).

- The source appears point-like in all bands except *i*-band where only the brighter pair of lensed images suggest extendedness in the tangential direction. This could suggest that we are detecting emission from the underlying AGN host galaxy. Alternatively, if there is no AGN, then the source (with  $r_{\text{eff}} \sim 0.2$  kpc) is one of the most compact galaxies at  $z \sim 4$ .

- We do not see any sign of variability in any of the four lensed images from the HSC data and VIKING *Z* and *Y*-bands except the VIKING *K*s-band data which show highly discrepant flux ratio for the brighter pair. The origin of the chromatic variation is not understood since none of the known phenomena such as intrinsic variability, microlensing and differential extinction can fully explain the measured optical and NIR flux ratios. We can not rule out microlensing due to lack of sufficient data.

In conclusion, the lensed source is most probably a low-luminosity AGN (LLAGN) but we can not exclude the possibility of it being a rare, highly compact bright galaxy.

If the source indeed has an AGN, then this represents the highest redshift quadruply lensed AGN. Conventionally, quasars (or bright AGNs) are favorable for cosmological studies as they are easier to follow-up on small telescopes for time-delay monitoring. However, LLAGNs also show variability, in fact, at much shorter time scales and the high redshift, quadruply lensed source of HSC J1152+0047 shows great promise for cosmological studies. Faint AGNs are also useful to study quasar fueling lifetime, feedback and faint end slope of the luminosity function (e.g., Hopkins et al. 2006; Glikman et al. 2010; Fiore et al. 2012; Ikeda et al. 2012; Matsuoka et al. 2016). Studying LLAGNs at high redshifts has been difficult due to their faintness and strong lensing might be the best means to study inner structures and mechanisms that drive the nuclear activity in distant LLAGNs.

Most of the surveys in the past have been shallow and wide enough to detect numerous lensed quasars (the brighter end of the AGN luminosity function). The discovery of HSC J1152+0047 from early HSC data demonstrates that HSC, with its unique combination of depth and wide imaging, is beginning to probe the fainter end of the AGN luminosity function. Looking ahead, we should expect to discover more lensed LLAGNs from HSC which will open a new avenue of studies. In the future, with even larger surveys such as the Large Synoptic Survey Telescope survey, lensed LLAGNs will probably be discovered routinely through variability.

## ACKNOWLEDGMENTS

AM is supported by World Premier International Research Center Initiative (WPI Initiative), MEXT, Japan. MO is supported by JSPS KAKENHI Grant Number 26800093 and 15H05892. S.H.S. is supported by the Max Planck Society through the Max Planck Research Group. S.H.S. and J.H.H.C. acknowledge support from the Ministry of Science and Technology in Taiwan via grant MOST-103-2112-M-001-003-MY3. A.S. acknowledges support by JSPS KAKENHI Grant Number 26800098. AM would like to thank T. Anguita, L. Hao, Y. Harikane, S. Huang, D. Sluse and M. Strauss for useful discussion. The authors would like to thank the referee for improving the presentation of the paper. The Hyper Suprime-Cam (HSC) collaboration includes the astronomical communities of Japan and Taiwan, and Princeton University. The HSC instrumentation and software were developed by the National Astronomical Observatory of Japan (NAOJ), the Kavli Institute for the Physics and Mathematics of the Universe (Kavli IPMU), the

University of Tokyo, the High Energy Accelerator Research Organization (KEK), the Academia Sinica Institute for Astronomy and Astrophysics in Taiwan (ASIAA), and Princeton University. Funding was contributed by the FIRST program from Japanese Cabinet Office, the Ministry of Education, Culture, Sports, Science and Technology (MEXT), the Japan Society for the Promotion of Science (JSPS), Japan Science and Technology Agency (JST), the Toray Science Foundation, NAOJ, Kavli IPMU, KEK, ASIAA, and Princeton University. This paper makes use of software developed for the Large Synoptic Survey Telescope. We thank the LSST Project for making their code available as free software at <http://dm.lsstcorp.org>. The Pan-STARRS1 Surveys (PS1) have been made possible through contributions of the Institute for Astronomy, the University of Hawaii, the Pan-STARRS Project Office, the Max-Planck Society and its participating institutes, the Max Planck Institute for Astronomy, Heidelberg and the Max Planck Institute for Extraterrestrial Physics, Garching, The Johns Hopkins University, Durham University, the University of Edinburgh, Queen's University Belfast, the Harvard-Smithsonian Center for Astrophysics, the Las Cumbres Observatory Global Telescope Network Incorporated, the National Central University of Taiwan, the Space Telescope Science Institute, the National Aeronautics and Space Administration under Grant No. NNX08AR22G issued through the Planetary Science Division of the NASA Science Mission Directorate, the National Science Foundation under Grant No. AST-1238877, the University of Maryland, and Eotvos Lorand University (ELTE). Based on observations obtained at the Gemini Observatory, which is operated by the Association of Universities for Research in Astronomy, Inc., under a cooperative agreement with the NSF on behalf of the Gemini partnership: the National Science Foundation (United States), the National Research Council (Canada), CONICYT (Chile), Ministerio de Ciencia, Tecnología e Innovación Productiva (Argentina), and Ministério da Ciência, Tecnologia e Inovação (Brazil). The authors wish to recognize and acknowledge the very significant cultural role and reverence that the summit of Mauna Kea has always had within the indigenous Hawaiian community. We are most fortunate to have the opportunity to conduct observations from this mountain. This research has made use of the NASA/IPAC Infrared Science Archive, which is operated by the Jet Propulsion Laboratory, California Institute of Technology, under contract with the National Aeronautics and Space Administration.

## REFERENCES

- Atek, H., et al. 2015, *ApJ*, 814, 69
- Axelrod, T., Kantor, J., Lupton, R. H., & Pierfederici, F. 2010, in *Proc. SPIE*, Vol. 7740, Software and Cyberinfrastructure for Astronomy, 774015
- Bouwens, R. J., et al. 2014, *ApJ*, 793, 115
- Bradley, L. D., et al. 2008, *ApJ*, 678, 647
- . 2014, *ApJ*, 792, 76
- Browne, I. W. A., et al. 2003, *MNRAS*, 341, 13
- Edge, A., Sutherland, W., Kuijken, K., Driver, S., McMahon, R., Eales, S., & Emerson, J. P. 2013, *The Messenger*, 154, 32
- Egami, E., et al. 2005, *ApJ*, 618, L5
- Elíasdóttir, Á., Hjorth, J., Toft, S., Burud, I., & Paraficz, D. 2006, *ApJS*, 166, 443
- Falco, E. E., et al. 1999, *ApJ*, 523, 617
- Fiore, F., et al. 2012, *A&A*, 537, A16



- Foreman-Mackey, D., Hogg, D. W., Lang, D., & Goodman, J. 2013, *PASP*, 125, 306
- Glikman, E., Bogosavljević, M., Djorgovski, S. G., Stern, D., Dey, A., Jannuzi, B. T., & Mahabal, A. 2010, *ApJ*, 710, 1498
- Glikman, E., Djorgovski, S. G., Stern, D., Dey, A., Jannuzi, B. T., & Lee, K.-S. 2011, *ApJ*, 728, L26
- Hashimoto, T., Ouchi, M., Shimasaku, K., Ono, Y., Nakajima, K., Rauch, M., Lee, J., & Okamura, S. 2013, *ApJ*, 765, 70
- Hopkins, P. F., Hernquist, L., Cox, T. J., Robertson, B., Di Matteo, T., & Springel, V. 2006, *ApJ*, 639, 700
- Huang, K.-H., et al. 2016, *ApJ*, 817, 11
- Ikeda, H., et al. 2012, *ApJ*, 756, 160
- Inada, N., et al. 2012, *AJ*, 143, 119
- Ivezic, Z., et al. 2008, *ArXiv e-prints*
- Jackson, N., Rampadarath, H., Ofek, E. O., Oguri, M., & Shin, M.-S. 2012, *MNRAS*, 419, 2014
- Jurić, M., et al. 2015, *ArXiv e-prints*
- Kobayashi, M. A. R., Totani, T., & Nagashima, M. 2010, *ApJ*, 708, 1119
- Magnier, E. A., et al. 2013, *ApJS*, 205, 20
- Malhotra, S., & Rhoads, J. E. 2002, *ApJ*, 565, L71
- Mason, R. E., Côté, S., Kissler-Patig, M., Levenson, N. A., Adamson, A., Emmanuel, C., & Crabtree, D. 2014, in *Proc. SPIE*, Vol. 9149, *Observatory Operations: Strategies, Processes, and Systems V*, 914910
- Matsuoka, Y., et al. 2016, *ApJ*, 828, 26
- Miralda-Escudé, J. 1998, *ApJ*, 501, 15
- Miyazaki, S., et al. 2012, in *Proc. SPIE*, Vol. 8446, *Ground-based and Airborne Instrumentation for Astronomy IV*, 84460Z
- More, A., et al. 2016, *MNRAS*, 456, 1595
- Myers, S. T., et al. 2003, *MNRAS*, 341, 1
- Oguri, M. 2010, *PASJ*, 62, 1017
- Oguri, M., et al. 2006, *AJ*, 132, 999
- Ouchi, M., et al. 2003, *ApJ*, 582, 60
- . 2008, *ApJS*, 176, 301
- . 2010, *ApJ*, 723, 869
- Parsa, S., Dunlop, J. S., McLure, R. J., & Mortlock, A. 2016, *MNRAS*, 456, 3194
- Peng, C. Y., Ho, L. C., Impey, C. D., & Rix, H.-W. 2002, *AJ*, 124, 266
- Planck Collaboration et al. 2016, *A&A*, 594, A13
- Rawle, T. D., et al. 2014, *ApJ*, 783, 59
- Richards, G. T., et al. 2001, *AJ*, 121, 2308
- . 2006, *AJ*, 131, 2766
- Riechers, D. A., Carilli, C. L., Walter, F., & Momjian, E. 2010, *ApJ*, 724, L153
- Rusu, C. E., et al. 2016, *MNRAS*, 458, 2
- Schlafly, E. F., et al. 2012, *ApJ*, 756, 158
- Schmidt, K. B., et al. 2016, *ApJ*, 818, 38
- Shibuya, T., Kashikawa, N., Ota, K., Iye, M., Ouchi, M., Furusawa, H., Shimasaku, K., & Hattori, T. 2012, *ApJ*, 752, 114
- Shibuya, T., Ouchi, M., & Harikane, Y. 2015, *ApJS*, 219, 15
- Sluse, D., Claeskens, J.-F., Hutsemékers, D., & Surdej, J. 2007, *A&A*, 468, 885
- Stark, D. P., Ellis, R. S., Richard, J., Kneib, J.-P., Smith, G. P., & Santos, M. R. 2007, *ApJ*, 663, 10
- Suyu, S. H., et al. 2016, *ArXiv e-prints*
- Tonry, J. L., et al. 2012, *ApJ*, 750, 99
- Treyer, M., & Wambsganss, J. 2004, *A&A*, 416, 19
- Wright, E. L., et al. 2010, *AJ*, 140, 1868